Cellulose (2025) 32:4573–4593
https://doi.org/10.1007/s10570-025-06521-y

ORIGINAL RESEARCH

Low-cost preparation of photocatalytic hydrolyzed cellulose composites, activated with one-step synthesized graphene oxide-metal oxide for dye degradation

Huseyin Gumus · Bulent Buyukkidan

Received: 4 December 2024 / Accepted: 27 March 2025 / Published online: 19 April 2025

Abstract In this study, a graphene oxide-metal oxide photocatalyst (GO-Mox) was prepared via a low-cost single-step carbonization process. The photocatalyst was mixed with hydrolyzed cellulose (Phc, derived from textile waste)-PVDF to obtain photocatalytic polymeric composites via nonsolvent-induced phase separation in dimethyl formamide (DMAc). The physicochemical and structural properties of the powder and composites were characterized by X-ray diffraction, scanning electron microscopy and Fourier transform infrared spectroscopy. Photoluminescence analysis and contact angle measurements were carried out. The photocatalytic properties of the composites were evaluated against the model pollutant methyl orange in the presence of air and H_2O_2 in batch systems. The highest decolorization and the removal capacity of kinetic calculations at equilibrium were 91.8% and 383 mg g^{-1} with Phc-30 respectively. The usability of composites as membrane materials was tested in the filtration cell. The flux and rejection percentage of Phc-20 were found as 42 L m^{-2} h^{-1} bar^{-1} and 73%, respectively. The Phc composites were found to be highly reusable and suitable as membrane materials with considerable dye removal performance and easy applicability.

Keywords Filtration · Graphene oxide · Photocatalysis · Hydrolyzed cellulose · Waste recycling

Introduction

Industrial activities that develop in parallel with the increasing world population are devastating to environmental components and, as a result, the scarcity of natural resources. The clean water scarcity is one of the most vital one of these problems. Petroleum and its derivatives from heavy industry, dye, medicine, pesticides and organic compound-based wastes are the most prominent pollutants that cause water pollution (Zhang et al. 2024). Controlled use and protection of natural resources are the main solutions. The purification of polluted water from organic, inorganic, toxic, carcinogenic and harmful components is the most common method known to prevent water scarcity (Hegab et al. 2022; Paul and Ahankari 2023).

Traditional water treatment methods such as adsorption, chemical oxidation or precipitation and bacterial treatment have been applied (Gunes et al.

Supplementary Information The online version contains supplementary material available at https://doi.org/10.1007/s10570-025-06521-y.

H. Gumus (✉)
Osmaneli Vocational School, Bilecik Seyh Edebali University, 11500 Osmaneli, Bilecik, Turkey
e-mail: huseyin.gumus@bilecik.edu.tr

B. Buyukkidan
Department of Chemistry, Kutahya Dumlupinar University, Kutahya, Turkey
e-mail: bulent.buyukkidan@dpu.edu.tr

2021). Each method has its own advantages with drawbacks, such as unsustainability, the need for multiple harsh chemicals, different reaction conditions, low regeneration and high costs (Rahimi et al. 2022). In the advanced oxidation process (AOP), many organic compounds and a wide variety of dye residues can be successfully degraded into carbon, water and other nontoxic compounds. Degradation is based on the chemical or photon activation of oxy, hydroxy or superoxide derivatives (Azimi-Fouladi et al. 2023). The crucial component of this method is photocatalytic heterogeneous semiconductors, in which the radical chain reaction is initiated by stimulating the electrons on the surface with proton exposure. TiO_2 or metal-TiO_2 composites prepared with different metal combinations are widely used due to their excellent photocatalytic activity, low cost and nontoxicity. In photocatalysis, light energy is converted into chemical energy, and these processes include the use of sustainable and eco-friendly solutions thanks to the use of reusable catalysts and wide light spectrum sensitivity as an energy source (Hani 2023). Many reactions, such as the removal of organic pollutants, hydrogen production, CO_2 reduction and antimicrobial applications, which are globally important issues, are carried out with high selectivity by using photocatalytic systems (Yang et al. 2021; Khader et al. 2023). In addition to being easily prepared by sol–gel, hydrothermal, microwave and solution mixing techniques, their light sensitivity makes photocatalysis more efficient than conventional catalytic processes. Studies aimed at increasing light absorption, shifting the absorption region, and obtaining the highest efficiency by increasing the surface area with various additives combined with TiO_2 are underway (Pestana et al. 2023; El Sammak et al. 2023). Because of the high charge recombination of TiO_2 and the wide band energy TiO_2 has been widely applied (Ismael 2020; Baiju et al. 2024). Titania compositions with different crystal forms (rutile, anatase) and different surface structures and particle sizes have also been synthesized by many routes, such as hydrothermal, sol–gel, solvothermal, vapor and electrochemical deposition and microwave and solution combustion methods (Ismael 2020).

After the discovery of its unique properties, such as chemical resistance, high electron transfer capacity and large surface area, the use of graphene in combination with TiO_2 has increased (Gomathi Devi and Kavitha 2016; Liu et al. 2023). Graphene is a valuable carbon derivative consisting of a single layer structure formed by carbon atoms that make sp^2 hybridizations. It is obtained from the graphite mineral, where these layers are bonded to each other with dipole forces. If graphite is separated into layers with oxidizing chemicals, a graphene oxide containing hydroxy and carboxyl groups is formed. If graphite is separated as a single layer without functional groups, it is called a graphene layer. Each structure has its own heat, electrical conductivity and physical strength (Mokhena et al. 2024). TiO_2-GO nano metal oxide doped Polyacrylonitrile (PAN)/β-cyclodextrin (β-CD) nanofiber membranes were tested for the removal of methylene blue (MB) and methyl orange (MO) dyes (10 mg L^{-1}) (Zhang et al. 2021). SiO_2 supported Ag_2O@CRA photocatalyst was prepared and tested for the degradation of 100 mL of 20 mg L^{-1} MB under 50W visible light. The photocatalytic activity of the powder photocatalyst proceeding via ·OH radicals was obtained 100% degradation under visible light irradiation for 60 min. (Adday and Al-Jubouri 2024). TiO_2-GO doped PVDF membranes were used for the removal of bovine serum albumin (BSA) (1 g L^{-1}) under UV irradiation for 120 min. Removal efficiencies of 8%, 46%, 53% and 80% were recorded for raw PVDF, GO, TiO_2 and TiO_2-GO doped membranes, respectively. Good integration of nanocomposites with polymer was effective in the formation of superior photocatalytic performance. In addition, photo degradation kinetics of TiO_2-GO modified membrane was recorded to be 108% faster than the TiO_2 doped membrane alone and 153% faster than the GO doped membrane alone (Xu et al. 2016). The catalyzing efficiencies of the composite membrane with TiO_2:GO mass ratio of 8:2 for 5 h under natural light were recorded as 93.52%. However, the high cost and environmental pollution resulting from the intense chemical requirements of the multistage process of obtaining GO and GO-TiO_2 limit the efficiency of these methods. Traditional pyrolysis conditions have time and energy-saving advantages, such as short reaction times and the ability to use chemicals in stoichiometric ratios in the preparation of graphene-TiO_2 combinations (Mishra et al. 2023). Methylene blue dye (10 ppm) filtration of TiO_2-GO anchored PVDF membranes was tested in non-irradiated and UV irradiated environments. The dye removal performances of raw, GO-PVDF and TiO_2-GO-PVDF

were recorded as 92.79%, 92.81% and 92.79%, respectively. However, the membrane flux at 2 bar operating pressure were recorded as 1.146, 4.476 and 7.770 L m^{-2} h^{-1}, respectively (Suriani et al. 2019). Catalytic polymeric composites are structures that provide easy separation from the reaction environment in addition to being reusable. They can perform light-controlled pollution removal, filtration and self-cleaning in a continuous flow system (Mazlan et al. 2024). Cellulosic structures are preferred composite materials because they can be obtained from biomass and waste and are biodegradable (Aydemir et al. 2023). These waste cellulose residues can be applied to obtain carboxymethyl cellulose, cellulose acetate and different chemicals. The use of micro and nanocellulose separated from biomass as composite materials is quite common (Gabryś et al. 2021; Saha et al. 2024). Textile wastes with high cotton content are an important source of cellulose, and those that cannot be used in the reweaving process are recycled only by burning. It is clear that separating micro and nanocellulose in textile wastes and converting them into fine chemicals such as cellulose composites, cellulose acetate and nitrocellulose will have significant environmental and economic benefits, in terms of bioconversion of waste materials (Liang et al. 2023; Taher et al. 2024).

In this study, a graphene oxide-TiO_2–Fe photocatalyst was synthesized in a single step via an environmentally friendly method under optimum pyrolysis conditions. The prepared low-cost powder composition was anchored to a polymer consisting of hydrolyzed cellulose (Phc, textile waste recycling product) and polyvinylidene fluoride (PVDF, added as a binder) to obtain a photocatalytic polymeric composite. The advantages of the catalyst preparation method and the activities of the powder and composites were evaluated considering various characterization techniques and methyl orange removal experiments. The dye removal data obtained in the presence of air and H_2O_2 with the batch process were applied to the Langmuir and Freundlich adsorption isotherms and the pseudo first- and pseudo second-order kinetic models. The filtration and rejection efficiency of the composite, which has the best physical and photocatalytic efficiency under light radiation, was tested in a cross-flow filtration cell. The feasibility of composites as a filtration membrane has been discussed by comparing its batch and filtration efficiencies. The reversible, irreversible and total fouling behaviors of composite membrane after 3 uses were calculated with the flux recovery ratio. This combination is important for waste recycling (i), preparation of photocatalyst composites for easy-low-cost recovery from the environment (ii), and most importantly, obtaining materials that can be used as filtration membranes (iii). Thus, the light sensitivities of the composites under batch and filtration conditions were analyzed in detail.

Materials

Waste textile remnants (TX, industrial grade) consisting of 80% cotton and 20% polyester were obtained from the Uşak Organized Industrial Zone, Turkey. Titanium (IV) isopropoxide, $Ti[OCH(CH_3)_2]_4$ (284.22 g mol^{-1}, 97% W/W, 0.960 g/mL), H_2SO_4 (98%), $FeCl_2.4H_2O$, (reagent plus ≥ 98%) sodium chloride, NaCl (58.44 g mol^{-1}), sodium hydroxide (NaOH ≥ 98%) and hydrochloric acid (HCl ≥ 37%), hydrogen peroxide (H_2O_2, 30% w/w) were all of analytical grade and were purchased from Sigma−Aldrich. Ethanol (C_2H_5OH ≥ 95%) was used for composite washing. Polyvinylidene fluoride (PVDF; Solef 6010) was used as the polymeric support with hydrolyzed cellulose. *N*,*N*-Dimethylformamide (DMF, 73.09 g mol^{-1}, 0.944 g/mL, analytical grade ≥ 99%, Sigma Aldrich) and distilled water were used as the solvent and phase separation liquid, respectively. Methyl orange (MO, Acid Orange 52, or Orange III) and graphite (G, +100 mesh) were purchased from Sigma and used without any further purification.

Synthesis of TiO_2

TiO_2 was synthesized according to our previous study (Gumus 2020). In brief, 50 mL of 0.1 mol/L titanium (IV) isopropoxide and 20 mL of NaCl (1% mass ratio) were mixed and stirred with a 300 rpm magnetic stirrer for 10 min. The resulting slurry was filtered and washed with hot ethanol and water to remove impurities. The precipitate was dried at 60 °C and ground to powder with a size of 50–80 µm after calcination at 500 °C for 1 h.

Synthesis of graphene oxide-metal oxide by carbonization

5 g of graphite was weighed and transferred into a 100 mL porcelain crucible. 50 mL distilled water was added, and the suspension was mixed. Powder TiO_2, 1:4 of the graphite, was added and ultrasonicated. Then, 0.5 mol/L $FeCl_2$ was added, where Fe was equal to the amount of TiO_2, and the mixture was ultrasonicated again. Fe was added to the composite to induce a highly effective photo Fenton process in the presence of photosensitive TiO_2. The prepared slurry was kept at 250 °C in a 5 mL/min N_2 atmosphere for 1 h. The mixture was then cooled and stored for analysis and incorporation into the polymer. The same procedure was repeated for comparison purposes with only graphite and graphene oxide-TiO_2 under the same conditions. The samples were named G (graphite), GO (graphene oxide obtained from carbonization of graphite), GO-TiO_2 and GO-TiO_2–Fe (graphene oxide-metal oxides, GO-Mox).

Preparation of graphene oxide-metal oxide-Phc composites

Hydrolyzed cellulose (Phc) was prepared according to our previous study (Gumus and Buyukkidan 2022). In brief, textile waste remnants were washed with ethanol. The samples were rinsed and dried at 60 °C for 24 h. 10 g of sample was mixed with sulfuric acid. Acid was added until a white slurry was obtained, after which the mixture was stirred at 45–55 °C for 1 h. Hydrolysis was completed by adding cold water, after which the slurry was allowed to settle. The mixture was washed and decanted until a neutral pH was reached. The white powder was dried at 60 °C and stored for later use in composite preparation.

10 g of dried hydrolyzed cellulose and PVDF were weighed and dissolved in DMF by ultrasonication to obtain a 14% mass ratio of hydrolyzed cellulose and PVDF to the solvent. Hydrolyzed cellulose and PVDF were mixed at a 1:1 ratio and stirred at 200 rpm at 65 °C for 4 h. Powder GO-TiO_2–Fe prepared by carbonization was added at 0, 5, 10, 20, and 30 mass% ratios to the polymer. PVDF was used as a support material due to its solubility similar to cellulose and homogeneous miscibility. For homogeneous dispersion, the polymer solution was ultrasonicated and stirred at 250 rpm for more than 2 h. The mixture was cast onto a flat surface (15 cm × 25 cm) with a 300 µm casting knife at 25 °C. After exposure to air for 10 s, the glass plate was quickly immersed in a coagulation bath. While the composites were dried for characterization, they were stored in distilled water for dye removal experiments. Composites containing 0, 5, 10, 20 and 30% GO-TiO_2–Fe in a 1:1 hydrolyzed cellulose/PVDF matrix were determined to be Phc, Phc-5, Phc-10, Phc-20 and Phc-30, respectively.

Characterization

The crystallinity of the powders and composites were investigated via X-ray diffraction (XRD; Rigaku 2000) at 40.0 kV, scanning range: 2°–80° and a 2°/min scanning speed with continuous scan mode. Powder and composite morphologies were imaged by scanning electron microscopy (SEM, Carl Zeiss ULTRA Plus) at 10 kV, aperture diameter: 9–10 µm, and scan speed: 7.7. For cross-sectional images, the samples were first broken in liquid nitrogen to obtain a better angle. Then, the sample was gold plated and fixed to a carbon holder. The distribution of graphene oxide-metal nanoparticles fixed on the Phc matrix was imaged with a Hitachi H 7650 transmission electron microscope (TEM) at 100 keV. Phc polymeric composites of 50 nm were placed on a copper grid using a microtome. The functional groups were determined by Perkin Elmer Fourier transform infrared (FT-IR) spectroscopy over the range of 4000–400 cm^{-1} at the number of 20 scans set automatically for best result. A photoluminescence spectrometer (Perkin Elmer FL6500, PV Instruments) was used to determine the electron−hole pair recombination of the powder and Phc composites. Absorbance data graphs were obtained against wavelength in the range of 200–900 nm with the Xe900 continuous xenon lamp. The surface areas of the samples were measured by a TriStar II 3020 Version 3.02 Brunauer–Emmett–Teller (BET) device. The analysis conditions are 10 s equilibrium time in N_2 adsorptive gas with 100 mmHg/min. evacuation rate. The results were calculated from the graphs of the amount of gas adsorbed against the relative pressure in g adsorbent with multi-point measurements. The water uptake capacity (WU%) of the composites was determined to obtain information about water absorption and pore distribution with porosity (PO%) values. For this purpose, composites stored in water were weighed (W_w)

after they were chopped slightly with blotting paper. The wet membranes were dried in a 40 °C vacuum oven for two hours, after which the composites were weighed again (W_d). The same experimental procedures were repeated 3 times for WU and PO% measurements. By using the wet and dry weights of the membranes, the water uptake capacities were calculated by Eq. (1) (Anadão et al. 2014).

$$WU(\%) = \frac{W_w - W_d}{W_w} \times 100 \quad (1)$$

The porosity percentages of the composites (PO%) were calculated by the weight of wet and dry membranes (Buonomenna et al. 2010) according to Eq. (2).

$$PO(\%) = \frac{W_w - W_d}{dA\delta} \times 100 \quad (2)$$

where d is the density of water used at 25 °C, A is the membrane area in the wet state (cm^2) and δ represents the thickness of the membrane in the wet form (cm). The change in the surface hydrophobicity of the composites was analyzed by contact angle (KSV Attention, Finland) at room temperature. The sessile drop method was used, and the average value of at least four measurements was calculated. Surface charge of powder Phc, Phc-20 and GO-TiO_2–Fe was measured by the zeta potential for five different pH ranges at 25 °C (Malvern Zatasizer Nano ZS-ZEN 3600 device). The results of the automatic 3-repeat measurement were obtained from the zeta potential (mV) versus total count graph.

Dye removal performance of Phc composites

A single-lamp photo reactor that has one 30 W of fluorescent blue light (15 × 287 mm, Philips, spectral range > 254 nm) was designed with a temperature-controlled stirrer. A schematic representation of the process is given in Fig. S1. The process involved the use of an aerator to adjust the temperature while maintaining uniform control. The photocatalytic efficiencies of the GO-TiO_2–Fe-doped composites were evaluated using an MO model organic dye, the physicochemical properties of which are given in Table S1. Phc composites were cut into 2 × 2 cm pieces and introduced into reaction vessels containing 50 mL of 50 mg/L MO. To establish adsorption equilibrium, the suspension containing the composites were mixed at 150 rpm in UV light turn-off mode. The amount of MO in the samples taken from the environment was analyzed at regular intervals. This process was continued until the difference in absorbance between the two samples was less than 1%. After adsorption equilibrium was established, the MO suspension was exposed to 30 W UV light from a distance of 15 cm for 30 min. H_2O_2 (0.01 mol/L) was added to the medium, and the same process was continued for 15 min. Experiments were repeated at least 3 times and the MO removal percentage was directly calculated from the MO absorbance using Eq. 3:

$$Removal(\%) = \left[\frac{C_0 - C_e}{C_0}\right] * 100 \quad (3)$$

where C_0 and C_e are the dye concentrations at the initial and equilibrium concentrations, respectively. Langmuir and Freundlich isotherms were generated with pseudo first- and pseudo-second-order kinetic models, respectively (Table S2). The dye removal performances of the composites were investigated in air and hydrogen peroxide as radical-forming reagents.

Filtration capabilities of the Phc composites

The pure water flux (PWF) performance of the Phc and Phc-20 membranes were measured in an ultrafiltration membrane cell (self-designed) and calculated in L m^{-2} h^{-1} bar^{-1} (Fig. S1). The filtration pressure (TMP) of the system was adjusted to 0.5, 1.5 and 2 bar after preconditioning the membrane for 3 h, and the PWF was calculated according to Eq. (4):

$$PWF = \frac{V}{At} \quad (4)$$

where V is the permeate volume (L), A is the membrane area (1.7×10^{-3} m^2) and t is the filtration time (h). The MO rejection performance of the membrane was tested in a filtration cell. Before the addition of the methyl orange solution, the pure water flux of the membranes was stabilized. 50 mg L^{-1} MO was pumped to filtration cell. Rejection values were calculated according to Eq. 3 for 30 min with 30 W of UV light turned off and on mode. Flux and rejection experiments were repeated at least 3 repetitions. Experiments were repeated with new membranes to

prevent performance reducing caused by using the same membrane.

Reusability and leaching studies

The reusability of the composites was evaluated after washing with 0.1 mol/L hydrochloric acid and distilled water. Photocatalytic studies were carried out as described in section "dye removal performance of Phc composites" and "filtration capabilities of the Phc composites" in batch and filtration system, respectively. Metal leaching was investigated by analyzing the water in which the composites were stored with reaction effluent using AAS (Perkin Elmer, PinAAcle 900 F).

The flux recovery ratio (FRR) of the membrane was calculated by Eq. 5.

$$\mathrm{FRR}(\%) = \left(\frac{\mathrm{PWF}_3}{\mathrm{PWF}_1}\right) \times 100 \tag{5}$$

The recycling performance of the membranes was evaluated via a 3-run filtration test with 3 repetitions by using new membranes. After washing with distilled water and measuring the fouled flux, the membrane was irradiated to degrade the contaminants. The reversible (R_r), irreversible (R_{ir}) and total fouling (R_t) rates were calculated by Eqs. 6–8 (Chen et al. 2021):

$$R_r(\%) = \left(1 - \frac{\mathrm{PWF}_2}{\mathrm{PWF}_1}\right) \times 100 \tag{6}$$

$$R_{ir}(\%) = \left(1 - \frac{\mathrm{PWF}_3}{\mathrm{PWF}_1}\right) \times 100 \tag{7}$$

$$R_t(\%) = \left(1 - \frac{\mathrm{PWF}_2}{\mathrm{PWF}_1}\right) \times 100 \tag{8}$$

where PWF_1 represents the pure water flux of the membrane in the first cycle. PWF_2 and PWF_3 are the fluxes of the membranes that had undergone MO filtration followed by water washing and UV irradiation, sequentially. In the filtration cell, the optimum concentration and experimental conditions determined via batch studies were used.

Results and discussion

Characterization of the powders and Phc composites

X-ray diffraction (XRD) was carried out to determine the changes in the crystallinity of the powders and Phc composites. High-angle XRD patterns of the powder and powder-anchored Phc are presented in Fig. 1. A broad maximum around of $2\Theta = 10°$ was observed in the XRD patterns of GO-TiO_2 and GO-TiO_2–Fe (Ouyang et al. 2013). The broad peak at $2\Theta = 10°$ proves that the graphite layers enlarged

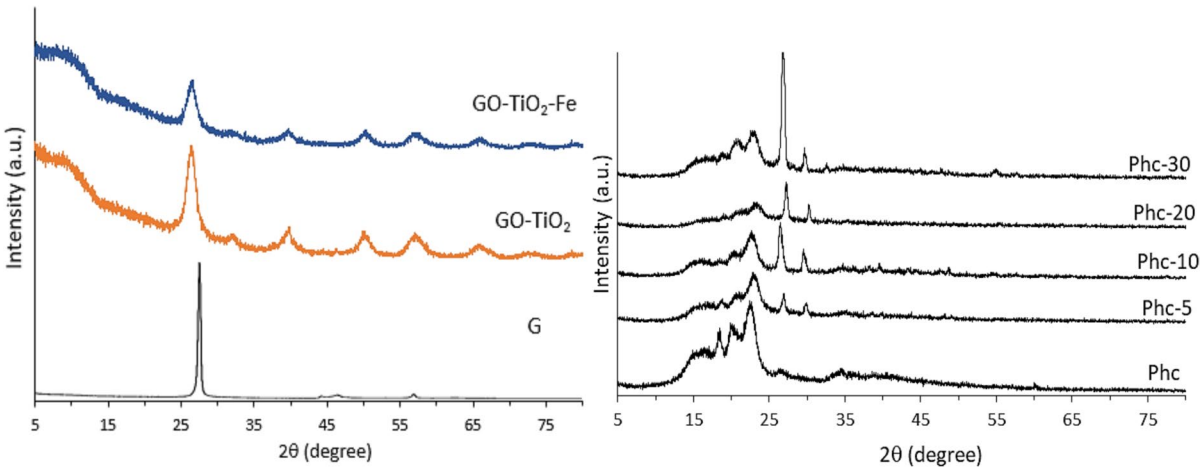

Fig. 1 XRD patterns of powders (left) and polymeric composites (right)

and turn into graphene oxide. In addition, the graphite peak showing the intercalation of graphite into graphene oxide at 2Θ = 27.6° shifted to 26.5° in carbonized GO-TiO_2 and GO-TiO_2–Fe. Unlike known graphene oxide preparation methods, a significant transformation of graphite into graphene oxide was obtained when the carbonization was applied (Ban et al. 2012). 2Θ = 25.39, 38.15, 48.37, 55.01, 69° and 2Θ = 31.07° which indicate that TiO_2 (Fig. S2) exists in the anatase and brookite phases respectively with high compatibility of JCPDS files Anatase:21-1272 (Ramakrishnan et al. 2012; Erusappan et al. 2021). These values were obtained as approximately 2Θ = 39.8, 50.1, 57.1 and 65.8° with small shifting in powder GO-TiO_2 and GO-TiO_2–Fe composites.

The homogeneous distribution of the polymers forming the composite in DMAc makes it difficult to determine the contribution of each component to the crystallinity. Compared with the diffraction patterns of raw cellulose and PVDF (Figs. S3 and S4), the distinct peaks observed in the crystal diffraction patterns of Phc composites at approximately 18º and 20º indicate the contribution of the alpha-phase PVDF (Ede et al. 2018). The contribution of cellulose to the crystal lattice of the composite is understood from the 22.7° peak in addition to peaks around 14–17°. The crystal structure of the Phc composite was very similar to that in our previous study contain cellulose (Gumus and Buyukkidan 2022). In the composites, starting from Phc-5, the 2Θ = 26.5° GO peak emerged. This value became most evident for Phc-30, which contained the highest amount of additive. Graphite was oxidized and exfoliated with Fe and turned into graphene oxide (as understood from the presence of the peak at approximately 2Θ = 10°). The low intensity of the GO peaks at around 2Θ = 10° proves that its' low crystallinity at exfoliated form. The XRD spectrum of the composite structure showed that the powder compressed the structure and the gaps between them were suppressed due to the presence of the additive and polymer. The intensity of the Phc peaks decreased and, the crystal structure becomes more amorphous with increasing additive amount. The peak at approximately 2Θ = 30° in all the Phc composites may be due to the Fe_3O_4 structure in the catalyst. Supporting this, the peaks at 2Θ = 35, 43 and 56.9° indicate the presence of FeO derivatives (Gumus 2019).

SEM and TEM images of the Phc composites are shown in Fig. 2. With the addition of TiO_2, graphite, which consists of combined layers, turned into a large-surface foam-like graphene oxide structure and GO-TiO_2 was obtained. Agglomeration occurred due to the iron species in the structure of the powder GO-TiO_2–Fe. The uniform distribution of the active metal catalyst on the polymer can be seen from the TEM image of Phc-20. Approximately spherical Fe nanoparticles with an average diameter of 42–45 nm were homogeneously anchored in the Phc. The iron-containing additives created large pores in the structure and caused partial compression in polymer. Fe is reduced by interacting with graphite during carbonization and releases acidic derivatives into the environment (Wu and Liu 2022). This effective redox exchange reshaped the catalyst structure.

A typical architecture with a selective top layer supported by a porous substructure was observed for the pristine Phc and Phc5-30 composites. The GO-TiO_2–Fe additive is more rigid and has narrower pores than the fluffy and swollen GO-TiO_2. According to the SEM analysis, the powder catalyst is homogeneously fixed to the polymeric structure. In the raw sample (Phc), the spongy and networked structure consisting of a wide and pure polymer gained a narrower and more complex appearance at Phc-5. An increase in the powder amount slowed the mass transfer rate during phase separation. The distance between the main lines decreased due to the increasing amount of additive ratio loaded into the polymer. Thus, the agglomeration increased with increasing additive ratio.

A detailed analysis of the molecular interactions between PVDF, Phc and the additive at different ratios via FT-IR is presented in Fig. 3. The bands at approximately 3400, 3024 and 2900 cm^{-1} are O–H stretching vibrations with the contribution of asymmetric CH_2 of PVDF and cellulose (Gumus and Buyukkidan 2022). The bands at 1400 and 1180 cm^{-1} and at 874 and 840 cm^{-1} represent the characteristic CH_2 rocking, C–C absorption, and CH and CF stretching vibrations of PVDF, respectively. In addition, C=O stretching vibrations together with C=C vibrations of Phc composites, originating from graphene oxide, were observed at approximately 1680 and 1733 cm^{-1} with very low intensity (Lee et al. 2021). The bands around 3400, 1700, 1634 and 1050 cm^{-1} seen in the IR spectrum of the powder catalyst formed as a result

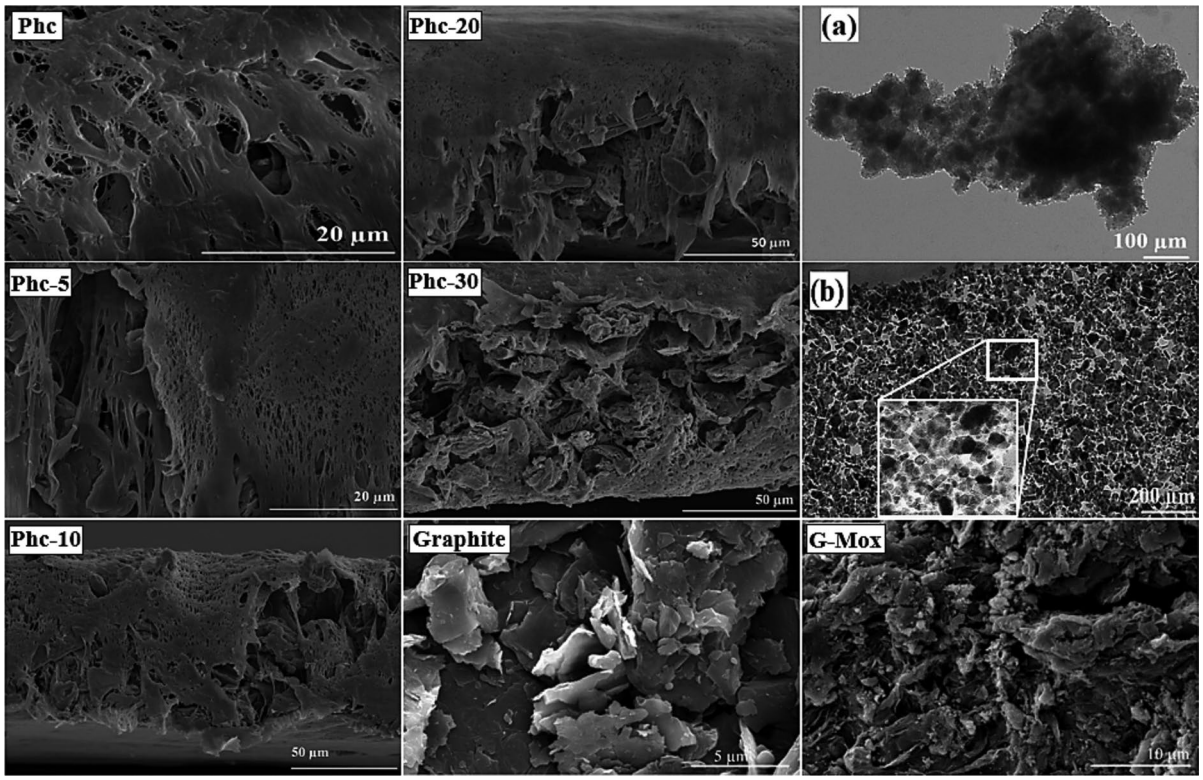

Fig. 2 SEM and TEM [**a** GO-TiO_2–Fe and **b** Phc-20] images of composites and powders

of carbonization belong to the OH, CO, C=C and C–O–C functional groups, respectively, indicating exfoliated graphene oxide layers (Kanta et al. 2017; Fig. S5). The existence of metal oxide structures interacting with C–O and CH groups is understood from the 500–850 cm^{-1} vibration bands.

The photoluminescence technique, which is based on the analysis of light emitted by excited electrons, is used to obtain information on the surface reactions of semiconductors (Fig. 4). The PL intensity is directly related to the electron–hole pair recombination. However, the higher the intensity is, the lower the photocatalytic activity, probably due to the long gap between the two bands. The electron–hole pair recombination and defect sites on the surface determine the efficiency of the semiconductor. When energy is supplied to a semiconductor, some electrons in the valence state are excited and move up to the conduction band. This results in empty places in the valence band, called "holes (h+)". The number of electrons and holes depends on how much energy is provided to the semiconductor. An electron is excited to the conduction band, which creates one hole in the valence band. This process is repeated for all electrons as much as the energy supplied. The holes formed in the valence band become positively charged. The hole and electron pair is called an "electron–hole" pair (Ramakrishnan et al. 2012). The high intensity was partially measured in the Phc composites because the polymer blocked the light. A high absorbance of raw Phc indicates a low photocatalytic effect.

Due to the high absorption of graphene oxide, GO-TiO_2 exhibited an absorbance at 650 nm in the visible region, as expected. The absorbance shifted to the near-infrared region for GO-TiO_2–Fe as a result of the addition of Fe to GO-TiO_2. The Phc-20 composite, prepared by anchoring GO-TiO_2–Fe to the polymer, exhibited different absorbances in three different regions. The absorbance at approximately 380 nm of Phc-20 proves that the Phc composites are suitable for use in photocatalysis in the presence of UV light.

The surface area, pore volume and pore diameter of the synthesized composites were determined via

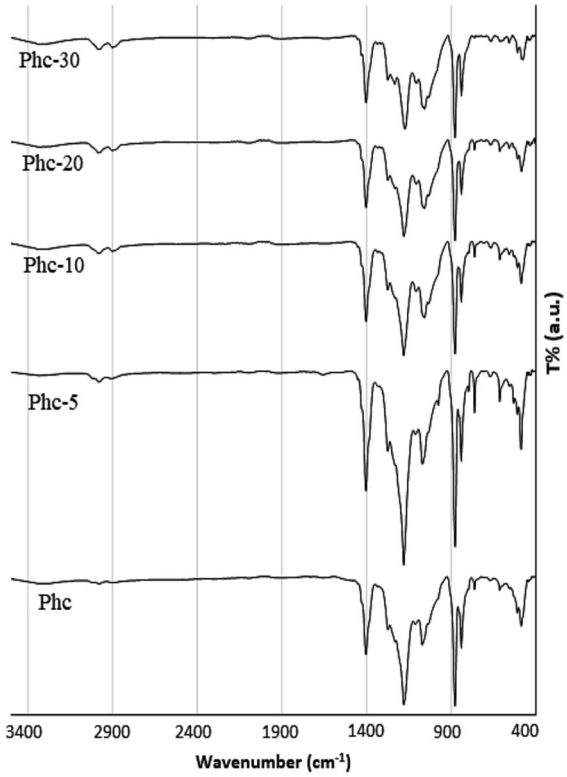

Fig. 3 FT-IR spectrums of Pch composites

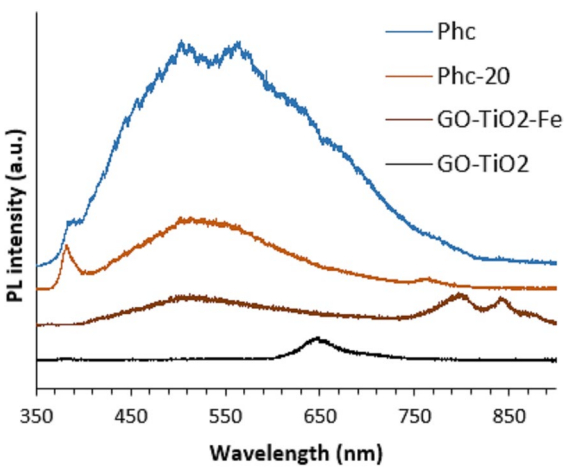

Fig. 4 Photoluminescence spectra of various catalysts

BET analysis (Table 1). The samples exhibited multiple types of isotherms with mixed-type hysteresis due to the mixture of meso and macropores. The surface areas of G, GO-TiO_2 and GO-TiO_2–Fe were measured as 2.3, 15.5 and 6.36 m^2/g, respectively. The surface area of the Phc composites increased with additive loading, and 13.4 m^2/g surface area was recorded for Phc-20. In polymer formation, thin-structured cellulose increases the surface area by effectively forming large pores. The GO-TiO_2–Fe addition resulted in a limited improvement in the surface area of Phc with an increased ratio. A remarkable increase in surface area was achieved with Phc-10 and Phc-20. With the amount of additive exceeding 20%, there was a shrinkage in the surface. As seen from the SEM images, this is because the 30% additive blocked the channels of the polymer support. A more meaningful result is obtained when the WU% and PO% of the composites are evaluated together with the surface area-pore volume and pore size. Although the total pore volume increased, the pore width decreased with increasing additive. The WU% and PO% values increased slightly. Specifically, while the pores narrow, many small spaces are still being created through water can enter. The small water retention capacity was due to the decreasing hydrophilicity of the graphene derivative.

An increase in the contact angle in proportion to the additive content of the Phc composites showed that the addition of GO-TiO_2–Fe increased the hydrophobicity (Table 1). The contact angle is an indicator of membrane wettability. Due to the presence of electronegative fluorine atoms which prone to form hydrogen bonds PVDF have led to partial hydrophilicity through the incorporation of highly hydrophilic hydrolyzed cellulose. However, the addition of the graphene oxide derivative gave the composite a partially hydrophobic feature due to the electronegative charges it contained. Despite the functional groups of graphene oxide, the exfoliated structure is randomly distributed in the polymer. Exfoliation could be inferred from changes in the XRD crystal structure and narrowing of the BET surface of GO-TiO_2–Fe. The groups are connected with each other or with the polymer chains, so they do not provide an effective hydrophilic property to the structure. This situation reduces the rate of H bonding between the composite and water molecules, thus reducing the interest of the structure in water and resulted with a small increase at hydrophobicity (Shah et al. 2019). However, the TiO_2 present in the structure prevents superhydrophobicity with hydrolyzed cellulose and ensures the stabilization of wettability. A highly hydrophilic

Table 1 BET surface area (S_{BET}), contact angle, water uptake%, and porosity% of the powders and Phc composites

Sample	SBET (m^2/g)	V_{total} (cm^3/g)	Pore width (nm)	Contact Angle (°)	WU%	PO%
G	2.30	0.022	5.4	–	–	–
GO-TiO_2	15.50	0.034	4.2	–	–	–
GO-TiO_2–Fe (G-Mo)	6.36	0.012	3.7	–	–	–
Phc	4.80	0.042	6.3	69.0 ± 0.7	59.2 ± 1.0	65.5 ± 0.7
Phc-5	5.10	0.008	5.5	72.5 ± 1.5	61.7 ± 0.3	66.0 ± 0.8
Phc-10	12.35	0.013	5.4	76.5 ± 0.3	66.5 ± 0.5	73.6 ± 0.7
Phc-20	13.40	0.017	5.1	79.0 ± 1.7	57.3 ± 0.2	72.8 ± 1.4
Phc-30	8.02	0.021	5.7	85.0 ± 1.0	55.9 ± 1.5	67.1 ± 1.2

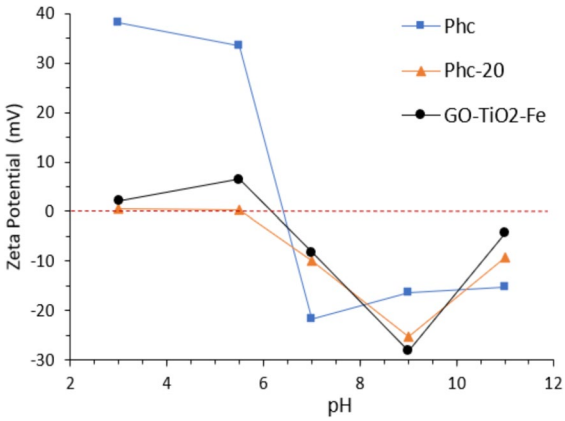

Fig. 5 Zeta potential curves of composites and GO-TiO_2–Fe

structure increases the efficiency of filtration or catalysis by facilitating the entry of water into pores. At the other hand, the hydrophobic structure makes the organic substrate reach its active areas easily. The Phc-5–30 composites exhibited optimal hydrophilic properties that were suitable for organic−inorganic substrates.

In order to determine the surface charges of Phc, Phc-20 and GO-TiO_2–Fe, their zeta potentials were measured (Fig. 5). The surface charge behaviors of the composites at different pHs are consistent with each other. The isoelectric point (IEP) value of Phc changed from 6.4 to 5.7 in Phc-20. Unlike raw GO (IEP:6.93), it was observed that the Fe–TiO_2 combined additive were effective for the determination of charge distribution of GO-TiO_2–Fe powder (Guo-Qiang et al. 2015; Saleem and Al-Jubouri 2024). The affinity of OH^- ions to the cationic surface provided the negative character. The IEP of the powder is 6.2 and it has quite anionic characteristics at higher pHs. It was understood that the surface behavior of GO-TiO_2–Fe was transferred to Phc-20. The surface of the composites and powder are negatively charged above pH:7 values that is the pH of the solution used in this study. At pH values lower than the IEP, the adsorption of negative ions will increase. However, it should be considered that the ions affected by the pH change and they will also be loaded with different charges.

Dye removal performance of composites

Adsorption

The dye removal performances of the composites were investigated in terms of adsorption and photocatalysis. For this, 50 mL (10–150 mg/L) of MO aqueous solution and 0.3 g of the composite were placed in a glass container and mixed at 150 rpm. Considering the acidic character of MO, we aimed to sequentially measure the activity of the photocatalyst at stable acidity by adjusting it to 7, which is an approximately neutral pH. The ambient temperature was kept constant at 25 °C, and adsorption continued until the UV analysis values of the two samples taken from the mixture were approximately equal. After equilibrium the dye mixture was subsequently placed in a UV light source (30 W, 254 nm wavelength) for 30 min. At the 30th minute, 0.01 mol/L H_2O_2 was added as a radical source, and UV treatment was carried out for 15 additional minutes under the same conditions. Thus, the dye removal performances of the composites were investigated in adsorption and photocatalytic systems sequentially in the presence of air and

hydrogen peroxide. Adsorption and photocatalysis results were evaluated independently of each other. Phc composites, whose adsorption and photocatalytic activities were tested in a batch system, are suitable materials for continuous filtration systems. Structures that are exposed to light and catalyze substrate accumulation on the surface are valuable alternative for impurity removal.

The dye removal performance of the composites increases slightly compared to that of the pristine Phc composite (Fig. 6). Cellulose-PVDF exhibited better adsorption than did raw cellulose and PVDF due to its characteristic absorption feature for 75 min. The additive incorporated in the structure of Phc improved the dye adsorption of the composite by increasing the pore structure and distribution. The dye adsorption capacities of Phc-10 and Phc-20 were 38.7% and 31.3%, respectively. The adsorption efficiency decreased with Phc-30, as the pressed structure prevented substrate transition. GO-TiO_2–Fe additive increased the Phc surface area after it was incorporated into the composite. Therefore, compared with that of the pristine form, the adsorption efficiency of the composites increased.

Effect of solution pH

The dye removal efficiencies of the composites at different pH values were investigated (Fig. 7a). Optimization studies were carried out with Phc-20, considering its physical properties and photocatalytic performance with Phc for comparison. No significant change was observed in either the adsorption or dye degradation efficiency in the pH range of 3–11. This difference may be the result of the similar surface properties of the MO and Phc composites in terms of electrostatic interactions. An increase in pH did not cause a change in either the adsorbent surface or the MO molecules. One of the most important parameters affecting adsorption is the particle charge in the aqueous solution (Choi et al. 2014). While the particle charge changes depending on the acidity/basicity of the environment, the surface charge of the adsorbent is also affected. It has been stated that dyestuffs and carbon derivatives may have amphoteric properties (Chiang et al. 2020). However, since cationic molecules become negatively charged at pH values greater than the IEP, this increases the effectiveness of the repulsive forces. Conversely, anionic structures become more positively charged after the isoelectric

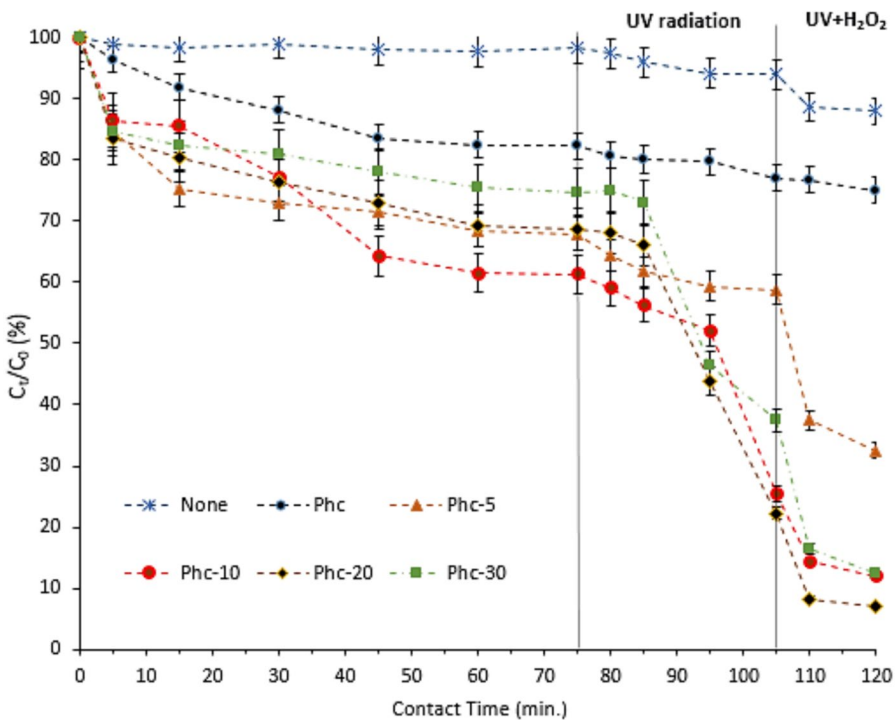

Fig. 6 MO removal (%) performances of composites in batch system (adsorbent dosage: 0.3 g, dye concentration and volume:50 mg/L and 50 mL, pH: 7.0, temperature: 298 K, 30W UV radiation for 30 min. (after 75th minute) and, UV radiation with one 30 W Xe lamp ($\lambda > 254$ nm) for 5 min. with 0.01 mol/L H_2O_2 (after 105th minute)

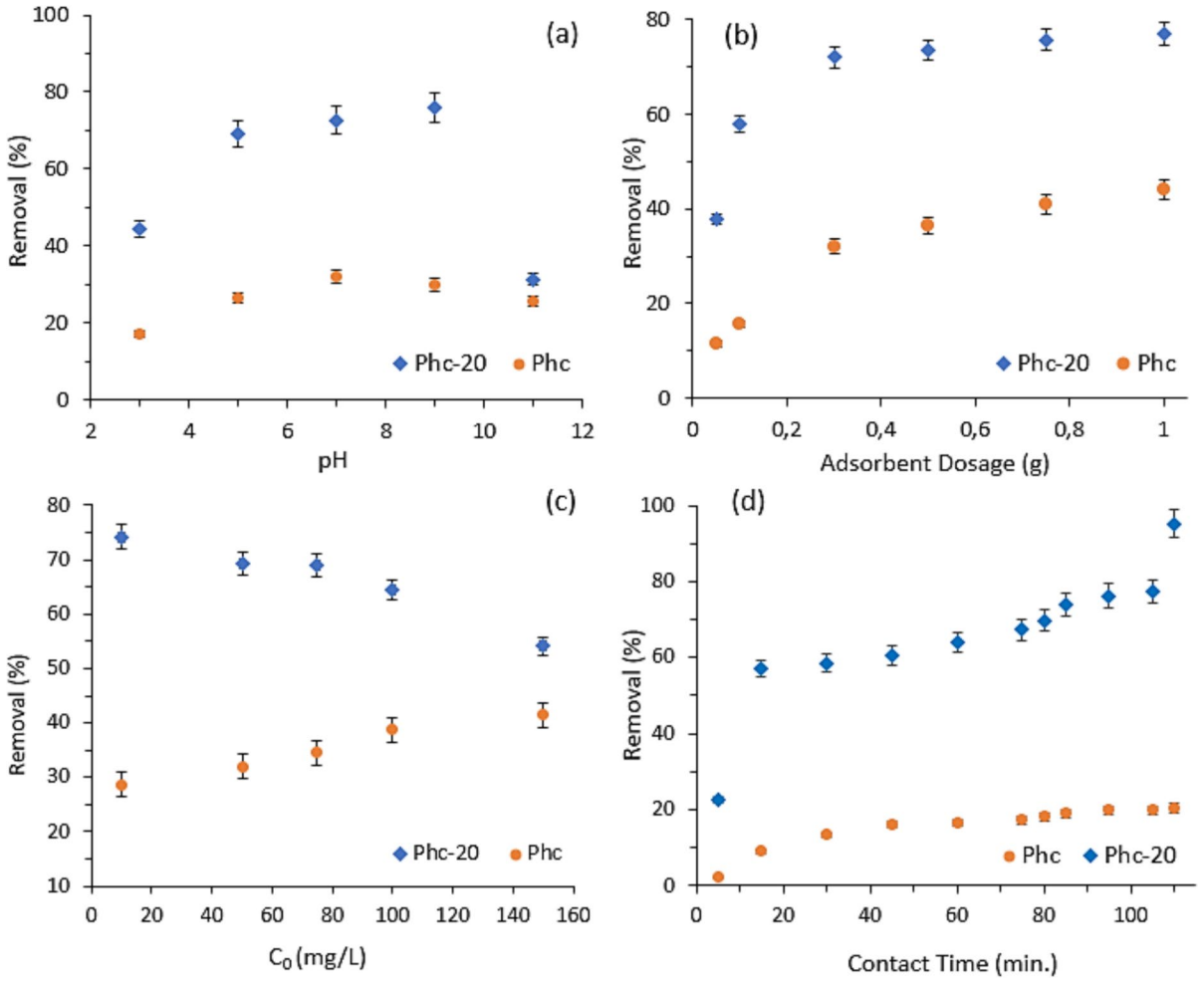

Fig. 7 Effect of pH (**a**), adsorbent dosage (**b**), initial MO concentration (**c**) and contact time (**d**) on the removal performance of Phc and Phc-20 composites. Optimum conditions = MO amount: 50 mL 50 mg/L, pH = 7.0, temperature: 298 K, adsorbent dosage: 0.3 g, stirring rate: 150 rpm, contact time for adsorption:75 min., one 30 W Xe lamp ($\lambda > 254$ nm)

pH is reached, and in both cases, the repulsive forces increase. Moreover, there was no significant change in the surface charge of the composites at different pH values. pH:7 is suitable for both MO molecules and the surface. A neutral pH will also be advantageous during filtration, and confusing efficiency differences due to acidity are prevented.

Effect of the adsorbent dosage

The effect of the adsorbent amount on the MO removal efficiency was investigated (Fig. 7b). All the experiments were performed as described in section "adsorption" with and without UV exposure. The composites were mixed for 75 min. to equilibrate, and analyses were performed at 10-min intervals. MO removal efficiency continued until the composite amount of 0.75 g. In order to better understand the MO removal mechanism of the composites, the adsorption behavior was examined with increasing composite amount without UV light. The composites were washed with 0.1 mol/L acidic and the MO amounts in effluent were analyzed again. Similar MO removal efficiency was exhibited in UV on and off modes with increasing composite amount. However, the MO amount in the photocatalyzed effluent was less. The results are discussed in detail in the section "Mineralization studies". As the adsorption efficiency

continued to increase with increasing amount, there was no significant change in MO removal by degradation. This is probably due to the adsorbed composite being protected from adequate light exposure with increasing amount. The increase in dye removal with increasing Phc amount was due to the adsorption of MO on Phc. This value is likely to increase at a nearly linear rate. However, dye removal efficiency by adsorption is lower than that by photocatalysis, and reusing of adsorbent composite may be more difficult and costly. This also proves that photocatalysis primarily occurs via adsorption. Moreover, due to the more compressed structure of Phc-20, the adsorption efficiency is lower than that of pristine Phc. Thus, Photocatalytic dye removal with Phc-20 is more convenient in every respect.

Effect of dye concentration and contact time

The effects of dye concentration and contact time on the dye removal efficiency of the composites are shown in Fig. 7c and d. Under the determined conditions, the removal efficiency first increased with increasing MO concentration and then stabilized. When the active areas to match the dye molecules in the environment were completed, the removal efficiency reached saturation. A higher removal ratio was obtained for photocatalysis than for adsorption. This is due to the degradation of the adsorbed molecules in the presence of light. A better dye removal efficiency was obtained at lower concentrations. This efficiency is an expected trend under dilute conditions, which are most suitable for free movement of particles. The degradation of molecules that can easily move to active areas under minimal repulsive forces decreased with increasing MO concentration. The contact time versus removal capacity compiled from the data in Fig. 6 are presented in Fig. 7d. The optimal time for MO adsorption equilibrium on the Phc composites was 75 min. It is estimated that adsorption and desorption are competitively effective due to equilibrium reactions occurring at longer contact times. Impurities on the surface were photocatalytically destroyed, the surface was cleaned, and the efficiency of the photocatalytic process stabilized over time. Light exposure after cleaning the surface of a composite has the potential to change the treatment efficiency.

The additive amount has a decisive effect on both the phase separation and adsorption performance. The interaction of each polymeric matrix with different additives is unique. For this reason, the physical and chemical properties of the composite, as well as its adsorption and catalytic performance, vary with different additive ratios. The optimum ratio of GO-TiO_2–Fe additive to the Phc structure was determined to be Phc-20 in terms of the composite structure and pollution removal performance. Adsorption data and initial MO concentrations were applied to the Langmuir and Freundlich isotherms (Fig. 8a) (Silva et al. 2018). Where C_e (mg/L), the equilibrium concentration of MO, Q_{max} is the maximum monolayer adsorption capacity of the composites, and K_f, n and K_L are the constants of the Langmuir and Freundlich isotherms, respectively.

Q_e is the adsorption capacity (mg/g) at equilibrium, and C_e is the dye concentration measured at equilibrium (Table 2). The isotherm data indicate that the adsorption of MO on the Phc composite occurred via monolayer adsorption on the homogeneous surface. It is also understood that the adsorption data are compatible with the Freundlich data. This is due to the increase in the roughness of the structure with the GO-TiO_2–Fe additive. The maximum adsorption capacity of 31.94 mg/g for Phc-30 was calculated at different initial concentrations. Considering the additive rate and removal percentage in the composite structure, the calculated values are quite reasonable. The total performance of the powder GO-TiO_2–Fe inside the composite was prevented due to the interaction of the powder with the polymer. However, compared with that of Phc, the MO removal of the Phc composites increased by approximately 79.1%.

Kinetic studies

The dye removal results of the composites were processed into pseudo first- and second-order kinetic models (Figs. 8b and S6). Here, Q_e is the adsorption/removal capacity (mg/g) at equilibrium; C_0 and C_e are the dye concentrations measured at initial and equilibrium; and Q_t is the adsorption/removal value reached at time t. The straight lines obtained from the t/Q_t and Q_t versus t graphs show that the kinetic model partially complies with the pseudo first order. The rate constants and Q_{max} obtained from each slope are given in Table 2. Among all the catalysts, Phc-30 had the highest Q_{max} value of 383 mg/g. Phc-30 showed the best dye removal performance among the

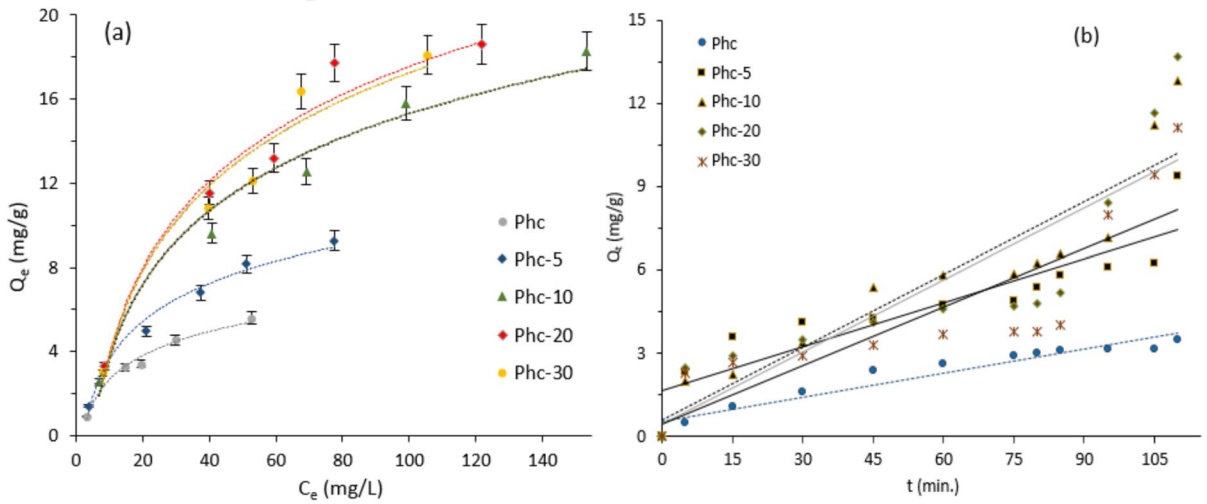

Fig. 8 Langmuir and Freundlich isotherms (**a**) with PSO kinetic graph (**b**) for MO removal on Phc composites (MO amount: 50 mL (10, 50, 75, 100 and 150 ppm), pH = 7.0, temperature: 298 K, adsorbent dosage: 0.3 g, stirring rate: 150 rpm for 110 min. one 30 W Xe lamp ($\lambda > 254$ nm)

Table 2 Adsorption and pseudo first order kinetic parameters of Phc composites for MO removal

	Langmuir isotherm			Freundlich isotherm			Pseudo first order kinetics			
	Q_{max} (mg/g)	K_L (L/mg)	R^2	K_f ($mg^{1-n}/g\ L^n$)	1/n	R^2	$Q_{e.exp}$ (mg/g)	k_1 (min^{-1})	$Q_{e.cal.}$ (mg/g)	R^2
Phc	8.32	0.03918	0.9892	0.4601	0.665	0.9718	3.722	0.02	3.6589	0.9939
Phc-5	13.29	0.02951	0.9968	0.625	0.646	0.9868	73.26	0.000765	71.65	0.8134
Phc-10	26.38	0.01446	0.9937	0.7685	0.652	0.9879	212	0.0000419	213	0.8623
Phc-20	29.41	0.01533	0.9594	0.8044	0.686	0.9713	344	0.000254	344	0.746
Phc-30	31.94	0.01291	0.9477	0.690	0.726	0.9838	383	0.000185	382	0.722

composites while the performances of Phc-10 and Phc-20 are nearly similar rate. The amount of active photocatalyst incorporated into the polymer determines the catalytic performance as far as the suitability of the composite structure. It was understood that 10 and 20% GO-TiO_2–Fe additive ratios were ideal values for obtaining photocatalytic composites considering physical structure and performance. This composition can be assumed the most favorable composition in terms of substrate transportation and other parameters.

Photocatalytic activity

The photocatalytic activities of the composites were evaluated based on the degradation of the MO model pollutant in a reactor with a single lamp. The sample, which reached adsorption equilibrium, was placed in a 30 W UV lamp at a distance of 15 cm and exposed to light first in air circulation and then in the presence of hydrogen peroxide. The dye removal percentages over time are given in Fig. 6. As a result of the reactions carried out in a catalyst-free environment (photolytic), no significant change was noted in the equilibrium concentration of MO. A decrease in the MO color was observed after adsorption in all the suspensions containing the Phc composites. This improvement occurred most clearly for Phc-10 and Phc-20. While the dye degradation in all the composites was slow in the presence of air oxygen, the reaction rate increased in the presence of hydrogen peroxide. The photocatalytic performance in air provided a more detailed understanding of the catalytic activities of

the composites. The efficiency of Phc-10 in the air environment, 74.45%, is at least as valuable as the high efficiency of Phc-20 and 30 in the peroxide environment. Phc-10 responded best to the oxidizer under air conditions. With the increase in oxidizing components created by the peroxide environment completely filling the active regions of Phc-10, the efficiency did not increase at the same rate. The active groups in the structure of Phc-20 were able to respond to high levels of peroxide and therefore showed high efficiency in a very short time. Hydrogen peroxide accelerated the formation of oxyl and hydroxyl radicals that decompose organic molecules by forming a peroxy metal complex with a metal oxide. The detailed mechanism for peroxy metal complex formation was described in our previous study (Gumus 2020; Gumus and Buyukidan 2024). By increasing the amount of Phc-10 in the suspension, an active site versus peroxide balance may be achieved. Phc-5, on the other hand, exhibited low efficiency due to the low number of oxidizing species it would encounter in both environments. The low capacity of Phc-30 is a result of the lower amount of UV light and substrate penetration due to the pressed structure of the composite with the highest additive amount. Photocatalysis was terminated after the effects of air and hydrogen peroxide were understood. Longer exposure to UV light could have catalyzed the entire substrate. In general, photocatalysis is based on radical formation from oxides, hydroxy groups or peroxide derivatives induced by conduction band electrons (e^-). The valence band (h^+) is an electron–hole pair formed by the light exposure. These radicals interact with the substrate and cause degradation of the target molecule (Gomathi Devi and Kavitha 2016; Zhang et al. 2019; Xiao et al. 2020; Zhao et al. 2023; González-Rodríguez et al. 2024). The formation of radicals through Fe derivatives is called the photo Fenton process. The rate and efficiency of the process mainly depend on the properties of the catalyst. Powder catalysts have relatively high yields, but the energy and chemicals required to separate them from solution are the greatest drawbacks. Polymeric composites with a catalyst fixed on their surface can be easily separated from the environment and can be used as filtration materials. The pore volume, hydrophilicity, pore distribution and durability, which determine the ability of a substrate to reach active surfaces, must be well adjusted. The active groups in the structure of the Phc composites promoted dye degradation by supporting radical formation at a certain rate.

Filtration efficiencies of the composites

To test the usability of the composites as membranes, the filtration performance was investigated under pressure conditions of 0.5, 1.5 and kPa. Phc-20 was placed in the filtration cell as a membrane since it has the best physical and photocatalytic performance at batch experiments. The membrane performance in terms of water flux and MO rejection is shown in Fig. 9. Phc had a better water flux than Phc-20. This is due to the more hydrophilic structure of the Phc composite. Despite the better porosity of Phc-20, the low water flux proves the presence of micro pores. This feature was effective in increasing the rejection performance of the membrane. The rejection test results performed with MO solution at a 50 mg/L concentration. The rejection performance of Phc-20 was 45%, while this value was 31% for Phc. This increase shows that the narrowed pore structure of the additive-containing composite results in better filtration.

With light exposure, the rejection performance changed significantly and it was 73% for Phc-20 at 0.5 bar transmembrane pressure with a

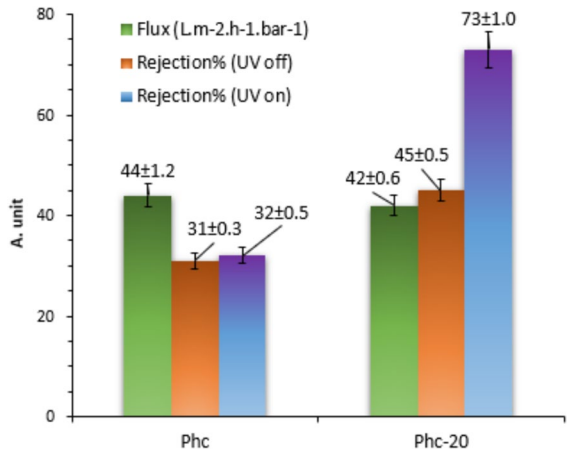

Fig. 9 Pure water flux performances of Phc and Phc-20. Flux conditions = membrane area: 1.7×10^{-3} m^2, 1000 mL 50 mg/L MO solution, transmembrane pressure = 0.5 bar, time of filtration = 0.5 h. one 30 W Xe lamp ($\lambda > 254$ nm)

42 L m^{-2} h^{-2} bar^{-1} flow rate. This increase is clearly due to the photocatalytic effect of the GO-TiO_2–Fe additive in the continuous-flow system. The photocatalytic performance of the composites recorded under batch conditions was also effective and proof the photocatalytic performance of composites in the filtration system. Reuse experiments were also conducted to determine whether light activation was effective at preventing pollution accumulation. First, the MO solution was filtered through to the membranes to obtain a constant flow. Then, the membrane was washed with pure water, UV irradiated for 1 h. FRR and fouling behaviors were calculated by equations [5–8] according to pure water fluxes of UV exposed membranes (Fig. 10). This cycle was repeated 3 times with same conditions. As shown in the figure, at the end of the third use, there was a significant decrease in the FRR value of Phc, while this value remained almost constant for the Phc-20 composite.

In addition, total fouling increased with the continuous uses of composite and partially decreased in the Phc-20 membrane. The photocatalytic effect reduced fouling and ensured that the breakdown of MO molecules accumulated on the surface. Since the impurities accumulated on the Phc surface could not be completely removed as a result of washing, the pores clogged, and flow loss occurred. The reversible fouling value of Phc-20 was greater than that of Phc. This result is directly related to the surface properties of Phc and Phc-20 determine the binding of MO to the surface. Compared to that on Phc, the reversible fouling on Phc-20 was greater due to greater MO adhesion because of its relatively more hydrophobic structure. Fortunately, due to the photocatalytic effect of Phc-20, total fouling was removed, and a decrease in the flux were prevented. The photocatalytic effect obtained in the batch system was adapted to the continuous flow system (Fig. 9). The self-cleaning performances of the membranes were tested. The Phc-20 composite is effective at removing surface impurities upon light exposure due to its photocatalytic sensitivity. Filtration with the Phc-20 structure is more advantageous than traditional filtration materials. The advantages of self-cleaning versus rejection performances under UV radiation at continuous flow system can be demonstrated with longer-term experiments. Rejection efficiency, wear behavior and energy efficiency can be investigated as the subject of another study.

According to the metal leaching analyses performed on the suspension collected after the third use, no metal was found within the limit of detection.

Mineralization studies

TOC analysis was performed to check whether the decolorization of dye was completely catalyzed. The decrease in carbon content of effluents after photocatalytic treatment is a clear indication of mineralization. Therefore, the contents of dye effluents collected after the photocatalytic reaction of Phc composites from the batch solution were analyzed (Table 3). The

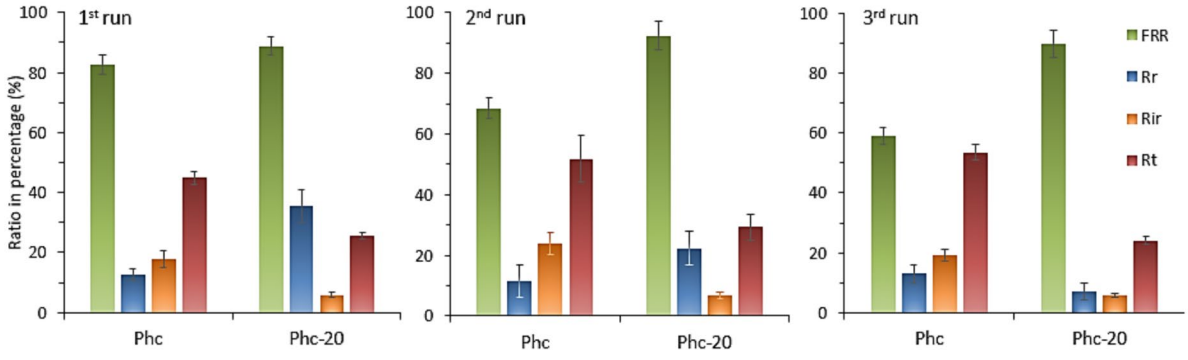

Fig. 10 Flux recovery ratio (FRR), reversible (Rr), irreversible (Rir) and total fouling ratio (Rt) of MO filtrated Phc and Phc-20 composite membranes during 3-run recycling process. Test conditions = membrane area: 1.7×10^{-3} m^2, 1000 mL 50 mg/L MO solution, conditioning pressure = 1 bar, transmembrane pressure = 0.5 bar, three consecutive steps of MO filtration (1st step), filtration after water washing (2nd step), and filtration after UV light irradiation (3rd step), time of washing = 5 min, time of light irradiation = 1 h, one 30 W Xe lamp ($\lambda > 254$ nm)

Table 3 Mineralization and decolorization percentages of MO on Phc composites

Sample	Decolorization (%)	Mineralization (%)
Phc	23.2	1.2
Phc-5	62.5	39.0
Phc-10	85.6	73.7
Phc-20	91.8	79.0
Phc-30	83.5	76.5

mineralization values are lower than the decolorization values. This difference may be due to the limited transformation of the dyestuff into colorless components (acetate, H_2O or CO_2) during catalysis. The color removal was due to adsorption of dye molecules or degradation of chromophore groups (Erusappan et al. 2021). An important advantage of this process is that a certain amount of color removal occurs via transformation in a very short time by the photocatalytic effect. A mineralization value parallel to the color removal was noted for the Phc composites.

A small amount of mineralization for Phc can be explained by the effect of light in a catalyst-free environment. The results show that the structure performs proportionally with increasing additive ratio anchored to polymer, but after 20% loading, performance decreased due to structural deformation. The variable performance values still indicate that dye removal by photocatalysis offers a more effective solution than adsorption. While decolorization is almost completely eliminated after desorption of adsorbed molecules, permanent color removal is achieved with photocatalysis. Different contact time, pH values, catalyst amount and other parameters may be effective on the mineralization% and could be studied in batch and filtration system.

Trapping experiments

Radical trapping/scavenging experiments were carried out simply to determine the most effective component in the catalysis process by trapping (Fig. 11). Methanol, TBA and ammonium oxalate were used as OH-SO_4, OH and h^+ quenchers, respectively. In the presence of the Phc-20 composite, photocatalysis of MO was nearly inhibited in methanol and TBA

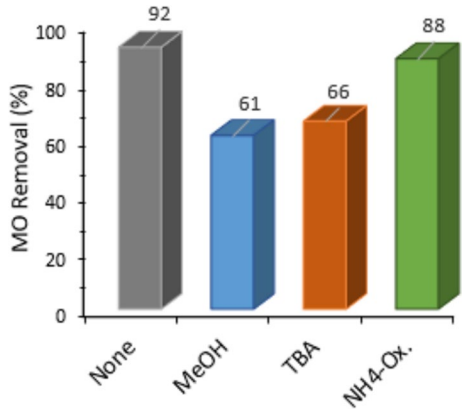

Fig. 11 Scavenging effect of MeOH, TBA and Ammonium Oxalate on MO degradation (0.3 g Phc-20 composite, pH:7, 15 mg/L MO, 0,01 mol/L H_2O_2, 20 min

media. It is understood that MO degradation is partially less affected by h^+ under these conditions.

OH radicals are the main component in MO photocatalysis with Phc composites (Xiao et al. 2020; González-Rodríguez et al. 2024). ·OH formation by light activation of hydrogen peroxide in the absence of catalyst is negligible. A small amount of radical formation was inferred in the presence of oxygen compared to that in the peroxide environment.

Recycling

In addition to the fouling experiments explained in the section "filtration efficiencies of the composites", the Phc-20 composite was tested for four consecutive photocatalytic runs to determine its durability and recycling performance in batch experiments. After each test, the composites were washed with 0.1 mol/L acidic solution and rinsed. The activity of the composites was slightly reduced (< 3%) after each use. Deterioration of the structure and blockage of the pores as a result of exposure to light caused a decrease in reuse efficiency and activity. As a result of the leaching studies conducted with calibration solutions of 1×10^{-3}–1×10^{-5} mol/L in the mixture, no metal ions were found in the eluents taken from the batch environment within the specified calibration ranges. In order to get knowledge about the molecular bonding of MO with the composite, IR spectra of Phc-20 after MO adsorption with UV and air oxygen are obtained in Fig. S7. Compared with the IR spectra

of the Phc composites (Fig. 3), the newly emerged band at approximately 1748 cm^{-1} corresponds to carbonyl derivatives as a result of the MO-Phc chain. This band clearly indicated to MO adsorption on the composite structure and is the most important stage for the catalytic process. It is possible that the radicals formed by light induction would primarily interact with the substrate adsorbed on the surface and located in the pores. The intensity of the characteristic bands of the polymer after adsorption generally decreased. This indicates that the crystallinity of the structure decreases and the amorphous structure increases as a result of the energy release and chemical formation occurring in the structure. The photocatalytic metal oxide-graphene oxide combination had synergistic effects on the MO degradation. MO-active site and peroxide-active site interactions are very rapid in a hydrogen peroxide environment compared with an oxygen environment. After separation of the composites, the suspension was exposed to UV radiation; however, there was no change in the concentration of MO.

Many studies have reported for removal of organic pollutants, pesticides and drug residues by using iron-graphene-doped polymeric composites as photocatalysts. Several studies in which impurities were catalyzed by photocatalysts under similar experimental conditions are reported in Table S3 (Gumus and Buyukidan 2024). Many parameters, such as the chemical structure of the photocatalyst, the properties of the substrate, the light intensity and the reaction time, directly affect the reaction efficiency. Composite catalysts not only retain their active structure but also regulate substrate retention and transformation via their channels. A composite with an appropriate channel and chemical structure increases the efficiency of the catalyst. In addition, these materials can be easily separated from the environment, and most importantly, they are candidates for use as filtration membranes. However, these materials have several disadvantages, such as high costs, low efficiency compared to powder structures, and surface wear due to higher light intensity. Phc composites are inexpensive and have acceptable performance for in situ dye and impurity degradation compared with the many results reported in the literature. In addition, with these features, Phc composites offer suitable alternatives to the clean production model required for a cleaner environment (Shi et al. 2021). Phc composites, the subject of this study, differ from those used in other studies in that they contain 50% waste cellulose and exhibit good photocatalytic effects when combined with low-cost graphene oxide-metal oxide photocatalysts. This was evident from the 91.8% removal of 50 mg/L MO in 25 mL in the presence of 0.3 g of catalyst under 30 W of light. An eco-friendly approach could be achieved by preparation of in situ membrane materials from waste for filtration.

Conclusions

GO-TiO_2–Fe-doped PVDF-Phc photocatalytic composites were prepared and tested for the photocatalytic removal of MO. XRD, SEM, BET and FT-IR techniques were used to analyze physical and molecular structures of composites. PL, contact angle, water uptake and porosity measurements were carried out with zeta potential. Graphite is transformed into graphene oxide under low-cost carbonization conditions which is effective at increasing the catalyst efficiency. The powder catalyst anchored to the Phc was effective on crystal structure of composite. With increasing solid-polymer ratio, a more compressed and narrow porous structure was formed. In terms of economic and functional considerations, the optimum GO-TiO_2–Fe additive ratio was obtained with Phc-20 according to the experimental results. According to consecutive adsorption and photocatalysis tests, the best overall efficiency was found to be 91.8% removal with Phc-20, while the best adsorption efficiency was found to be 38.7% with Phc-10. The filtration and fouling performances of the Phc-20 membrane were compared with those of the Phc. While high flux performance was achieved due to the hydrophilic nature of Phc, the MO rejection capacity, FRR and fouling resistance of Phc-20 were found to be noticeably greater due to its photocatalytic feature. The efficiency of Phc-20 in the presence of light in batch and filtration tests was quite satisfactory compared to that of other compositions. From the mineralization and decoloration results, it was understood that some of the dye removal may be due to the effective degradation of MO, while some may be due to its transformation into colorless molecules. Increasing contact angle values with increasing additive ratio indicate that the composite has the potential to effectively catalyze the photocatalysis of organic substrates.

Considering their abilities of to be reused for three runs, easy separation from the reaction environment and low cost, Phc composites are environmentally friendly structures obtained from recycled materials.

Author contributions All the authors contributed to the study conception and design. Material preparation, data collection and analysis were performed by Huseyin Gumus and Bulent Buyukkidan. The first draft of the manuscript was written by Huseyin Gumus, and all the authors commented on previous versions of the manuscript. All the authors read and approved the final manuscript.

Funding Open access funding provided by the Scientific and Technological Research Council of Türkiye (TÜBİTAK). This work has been supported by Kütahya Dumlupınar University Scientific Research Projects Coordination Office under grant number 2023-25.

Data availability All datasets were given as raw and/or interpreted in this study and in the supplementary materials. XRD, FT-IR, zeta and PL graphs were created directly using raw analysis data (Gumus and Buyukkidan 2024).

Declarations

Conflict of interest The authors declare that they have no conflicts of interest.

References

Adday AS, Al-Jubouri SM (2024) Photocatalytic oxidative removal of the organic pollutant from wastewater using recyclable Ag_2O@CRA heterojunction photocatalyst. Case Stud Chem Environ Eng 10:100852. https://doi.org/10.1016/j.cscee.2024.100852

Anadão P, Sato LF, Montes RR, De Santis HS (2014) Polysulphone/montmorillonite nanocomposite membranes: effect of clay addition and polysulphone molecular weight on the membrane properties. J Membr Sci 455:187–199. https://doi.org/10.1016/j.memsci.2013.12.081

Aydemir D, Sözen E, Borazan I et al (2023) Electrospinning of PVDF nanofibers incorporated cellulose nanocrystals with improved properties. Cellulose 30:885–898. https://doi.org/10.1007/s10570-022-04948-1

Azimi-Fouladi A, Falak P, Hassanzadeh-Tabrizi SA (2023) The photodegradation of antibiotics on nano cubic spinel ferrites photocatalytic systems: a review. J Alloys Compd 961:171075. https://doi.org/10.1016/j.jallcom.2023.171075

Baiju S, Masuda U, Datta S et al (2024) Photo-electrochemical green-hydrogen generation: fundamentals and recent developments. Int J Hydrogen Energy 51:779–808. https://doi.org/10.1016/j.ijhydene.2023.10.210

Ban FY, Majid SR, Huang NM, Lim HN (2012) Graphene oxide and its electrochemical performance. Int J Electrochem Sci 7:4345–4351. https://doi.org/10.1016/S1452-3981(23)19543-5

Buonomenna MG, Golemme G, Figoli A, Drioli E (2010) Fluorinated membranes as interfaces for application in catalysis. Desalination 250:1147–1149. https://doi.org/10.1016/j.desal.2009.09.129

Chen Z, Chen G-E, Xie H-Y et al (2021) Photocatalytic antifouling properties of novel PVDF membranes improved by incorporation of SnO_2-GO nanocomposite for water treatment. Sep Purif Technol 259:118184. https://doi.org/10.1016/j.seppur.2020.118184

Chiang C-H, Chen J, Lin J-H (2020) Preparation of pore-size tunable activated carbon derived from waste coffee grounds for high adsorption capacities of organic dyes. J Environ Chem Eng 8:103929. https://doi.org/10.1016/j.jece.2020.103929

Choi G-G, Jung S-H, Oh S-J, Kim J-S (2014) Total utilization of waste tire rubber through pyrolysis to obtain oils and CO_2 activation of pyrolysis char. Fuel Process Technol 123:57–64. https://doi.org/10.1016/j.fuproc.2014.02.007

Ede SR, Anantharaj S, Subramanian B et al (2018) Microwave-assisted template-free synthesis of $Ni_3(BO_3)_2$(NOB) hierarchical nanoflowers for electrocatalytic oxygen evolution. Energy Fuels 32:6224–6233. https://doi.org/10.1021/acs.energyfuels.8b00804

El Sammak AA, Mohamed WAA, Elnaggar EM, El-Sayed BA (2023) Recycling and photodegradation processes of organic hazardous materials on polyaniline-titanium dioxide quantum dots catalyst. Egypt J Pet 32:15–23. https://doi.org/10.1016/j.ejpe.2023.07.002

Erusappan E, Thiripuranthagan S, Radhakrishnan R et al (2021) Fabrication of mesoporous TiO_2/PVDF photocatalytic membranes for efficient photocatalytic degradation of synthetic dyes. J Environ Chem Eng 9:105776. https://doi.org/10.1016/j.jece.2021.105776

Gabryś T, Fryczkowska B, Biniaś D et al (2021) Preparation and properties of composite cellulose fibres with the addition of graphene oxide. Carbohydr Polym 254:117436. https://doi.org/10.1016/j.carbpol.2020.117436

Gomathi Devi L, Kavitha R (2016) A review on plasmonic metalTiO_2 composite for generation, trapping, storing

and dynamic vectorial transfer of photogenerated electrons across the Schottky junction in a photocatalytic system. Appl Surf Sci 360:601–622. https://doi.org/10.1016/j.apsusc.2015.11.016

González-Rodríguez J, Conde JJ, Vargas-Osorio Z et al (2024) LED-driven photo-Fenton process for micropollutant removal by nanostructured magnetite anchored in mesoporous silica. J Environ Manag 349:119461. https://doi.org/10.1016/j.jenvman.2023.119461

Gumus H (2019) Performance investigation of Fe_3O_4 blended poly (vinylidene fluoride) membrane on filtration and benzyl alcohol oxidation: evaluation of sufficiency for catalytic reactors. Chin J Chem Eng 27:314–321. https://doi.org/10.1016/j.cjche.2018.05.006

Gumus H (2020) Catalytic performance of polyvinylidene fluoride (PVDF) supported TiO_2 additive at microwave conditions. J Turk Chem Soc Sect Chem 7:361–374. https://doi.org/10.18596/jotcsa.610886

Gumus H, Buyukkidan B (2024) A facile preparation of biochar-anchored magnetic photocatalytic PVDF composite for water remediation. Colloid Polym Sci 302:103–115. https://doi.org/10.1007/s00396-023-05177-z

Gumus H, Buyukkidan B (2022) Physicochemical properties and adsorption performances of textile waste based hydrolyzed cellulose-PVDF composites. Rev Roum Chim 67:197–205. https://doi.org/10.33224/rrch.2022.67.3.08

Gumus H, Buyukkidan B (2024) Easily prepared graphene anchored PVDF-hydrolized cellulose photocatalytic composite. Mendeley Data, V1, https://doi.org/10.17632/6s8km8w452.1

Gunes K, Masi F, Ayaz S et al (2021) Domestic wastewater and surface runoff treatment implementations by constructed wetlands for Turkey: 25 years of experience. Ecol Eng 170:106369. https://doi.org/10.1016/j.ecoleng.2021.106369

Guo-Qiang L, Fu-Zhi S, Yao-Gang L et al (2015) Preparation and electrical properties of graphene coated glass fiber composites. J Inorg Mater 30:763. https://doi.org/10.15541/jim20140686

Hani U (2023) Comprehensive review of polymeric nanocomposite membranes application for water treatment. Alex Eng J 72:307–321. https://doi.org/10.1016/j.aej.2023.04.008

Hegab HM, Kallem P, Pandey RP et al (2022) Mechanistic insights into the selective mass-transport and fabrication of holey graphene-based membranes for water purification applications. Chem Eng J 431:134248. https://doi.org/10.1016/j.cej.2021.134248

Ismael M (2020) Enhanced photocatalytic hydrogen production and degradation of organic pollutants from Fe (III) doped TiO_2 nanoparticles. J Environ Chem Eng 8:103676. https://doi.org/10.1016/j.jece.2020.103676

Kanta U, Thongpool V, Sangkhun W et al (2017) Preparations, characterizations, and a comparative study on photovoltaic performance of two different types of graphene/TiO_2 nanocomposites photoelectrodes. J Nanomater 2017:1–13. https://doi.org/10.1155/2017/2758294

Khader EH, Mohammed TJ, Albayati TM et al (2023) Current trends for wastewater treatment technologies with typical configurations of photocatalytic membrane reactor hybrid systems: a review. Chem Eng Process Process Intensif 192:109503. https://doi.org/10.1016/j.cep.2023.109503

Lee J-E, Shin Y-E, Lee G-H et al (2021) Polyvinylidene fluoride (PVDF)/cellulose nanocrystal (CNC) nanocomposite fiber and triboelectric textile sensors. Compos Part B Eng 223:109098. https://doi.org/10.1016/j.compositesb.2021.109098

Liang J, Zhang P, Zhang R et al (2023) Bioconversion of volatile fatty acids from organic wastes to produce high-value products by photosynthetic bacteria: a review. Environ Res 242:117796

Liu H, Wang K, Zhang D et al (2023) Adsorption and catalytic removal of methyl orange from water by PIL-GO/TiO_2/Fe_3O_4 composites. Mater Sci Semicond Process 154:107215. https://doi.org/10.1016/j.mssp.2022.107215

Mazlan NA, Lewis A, Chen Z et al (2024) Photocatalytic self-cleaning graphene oxide/ZnO hybrid membrane for ultrafast cyclic small organic molecule separation. J Membr Sci 697:122539. https://doi.org/10.1016/j.memsci.2024.122539

Mishra A, Verma V, Khan A et al (2023) Waste ilmenite sludge-derived low-cost mesoporous Fe-doped TiO_2: a versatile photocatalyst for enhanced visible light photocatalysis without a cocatalyst. J Environ Chem Eng 11:110319. https://doi.org/10.1016/j.jece.2023.110319

Mokhena TC, Mochane MJ, Mtibe A et al (2024) Recent advances on nanocellulose-graphene oxide composites: a review. Cellulose 31:7207–7249. https://doi.org/10.1007/s10570-024-06055-9

Ouyang W, Sun J, Memon J et al (2013) Scalable preparation of three-dimensional porous structures of reduced graphene oxide/cellulose composites and their application in supercapacitors. Carbon 62:501–509. https://doi.org/10.1016/j.carbon.2013.06.049

Paul J, Ahankari SS (2023) Nanocellulose-based aerogels for water purification: a review. Carbohydr Polym 309:120677. https://doi.org/10.1016/j.carbpol.2023.120677

Pestana CJ, Hui J, Camacho-Muñoz D et al (2023) Solar-driven semi-conductor photocatalytic water treatment (TiO_2, g-C_3N_4, and TiO_2+g-C_3N_4) of cyanotoxins: proof-of-concept study with microcystin-LR. Chemosphere 310:136828. https://doi.org/10.1016/j.chemosphere.2022.136828

Rahimi SM, Panahi AH, Moghaddam NSM et al (2022) Breaking down of low-biodegradation Acid Red 206 dye using bentonite/Fe_3O_4/ZnO magnetic nanocomposite as a novel photo-catalyst in presence of UV light. Chem Phys Lett 794:139480. https://doi.org/10.1016/j.cplett.2022.139480

Ramakrishnan R, Kalaivani S, Amala Infant Joice J, Sivakumar T (2012) Photocatalytic activity of multielement doped TiO_2 in the degradation of congo red. Appl Surf Sci 258:2515–2521. https://doi.org/10.1016/j.apsusc.2011.10.085

Saha S, Ghosh G, Mondal D, Chakraborty S (2024) Efficacy of cellulose nanocrystals fabricated from *Crotalaria juncea* as novel adsorbent for removal of cationic dyes. Sādhanā 49:68. https://doi.org/10.1007/s12046-023-02410-x

Saleem AG, Al-Jubouri SM (2024) Separation performance of cationic and anionic dyes from water using polyvinylidene

fluoride-based ultrafiltration membrane incorporating polyethylene glycol. Desalin Water Treat 319:100546. https://doi.org/10.1016/j.dwt.2024.100546

Shah LA, Malik T, Siddiq M et al (2019) TiO_2 nanotubes doped poly(vinylidene fluoride) polymer membranes (PVDF/TNT) for efficient photocatalytic degradation of brilliant green dye. J Environ Chem Eng 7:103291. https://doi.org/10.1016/j.jece.2019.103291

Shi L, Liu J, Wang Y, Chiu A (2021) Cleaner production progress in developing and transition countries. J Clean Prod 278:123763. https://doi.org/10.1016/j.jclepro.2020.123763

Silva TL, Cazetta AL, Souza PSC et al (2018) Mesoporous activated carbon fibers synthesized from denim fabric waste: efficient adsorbents for removal of textile dye from aqueous solutions. J Clean Prod 171:482–490. https://doi.org/10.1016/j.jclepro.2017.10.034

Suriani AB, Muqoyyanah MA et al (2019) Incorporation of electrochemically exfoliated graphene oxide and TiO_2 into polyvinylidene fluoride-based nanofiltration membrane for dye rejection. Water Air Soil Pollut 230:176. https://doi.org/10.1007/s11270-019-4222-x

Taher MN, Al-Mutwalli SA, Barisci S et al (2024) Progress on remediation of per- and polyfluoroalkyl substances (PFAS) from water and wastewater using membrane technologies: a review. J Water Process Eng 59:104858. https://doi.org/10.1016/j.jwpe.2024.104858

Wu Y, Liu B (2022) $Mg(NO_3)_2{\cdot}6H_2O$-modified porous carbon derived from peanut shell: formation mechanism and efficient removal of p-nitrophenol. React Kinet Mech Catal 135:2085–2098. https://doi.org/10.1007/s11144-022-02212-y

Xiao R, He L, Luo Z et al (2020) An experimental and theoretical study on the degradation of clonidine by hydroxyl and sulfate radicals. Sci Total Environ 710:136333. https://doi.org/10.1016/j.scitotenv.2019.136333

Xu Z, Wu T, Shi J et al (2016) Photocatalytic antifouling PVDF ultrafiltration membranes based on synergy of graphene oxide and TiO_2 for water treatment. J Membr Sci 520:281–293. https://doi.org/10.1016/j.memsci.2016.07.060

Yang J, Song H, Zhang Y, Zhu X (2021) Preparation of functionalization graphite carbonitride photocatalytic membrane and its application in degradation of organic pollutants. Surf Interfaces 24:101092. https://doi.org/10.1016/j.surfin.2021.101092

Zhang H, Zhang C, Zhang Y et al (2019) P/N co-doped carbon derived from cellulose: a metal-free photothermal catalyst for transfer hydrogenation of nitroarenes. Appl Surf Sci 487:616–624. https://doi.org/10.1016/j.apsusc.2019.05.144

Zhang R, Ma Y, Lan W et al (2021) Enhanced photocatalytic degradation of organic dyes by ultrasonic-assisted electrospray TiO_2/graphene oxide on polyacrylonitrile/β-cyclodextrin nanofibrous membranes. Ultrason Sonochem 70:105343. https://doi.org/10.1016/j.ultsonch.2020.105343

Zhang Q, Zheng W, Zhang H et al (2024) Occurrence, fate and distribution of emerging organic pollutants in full-scale hybrid constructed wetlands treating municipal effluents. J Water Process Eng 61:105291. https://doi.org/10.1016/j.jwpe.2024.105291

Zhao F, Yang Y, Ji S et al (2023) Photocatalysis-Fenton mechanism of rGO-enhanced Fe-doped carbon nitride with boosted degradation performance towards rhodamine B. J Water Process Eng 55:104080. https://doi.org/10.1016/j.jwpe.2023.104080